High thermoelectric performance of aluminum-doped cuprous selenide thin films with exceptional flexibility for wearable applications

Dong Yang, Dongliang Zhang, Dongwei Ao, Mohammad Nisar, Adil Mansoor, Yuexing Chen, Li Fu, Hongli Ma, Guangxing Liang, Xianghua Zhang, et al.

High thermoelectric performance of aluminum-doped cuprous selenide thin films with exceptional flexibility for wearable applications

Dong Yang [a, b], Dongliang Zhang [a], Dongwei Ao[c], Mohammad Nisar [a], Adil Mansoor [a], Yuexing Chen [a], Li Fu [a], Hongli Ma [b], Guangxing Liang [a], Xianghua Zhang [b], Ping Fan [a], Zhuanghao Zheng [a,*]

a Shenzhen Key Laboratory of Advanced Thin Films and Applications, Key Laboratory of Optoelectronic Devices and Systems of Ministry of Education and Guangdong Province, College of Physics and Optoelectronic Engineering, Shenzhen University, Shenzhen, Guangdong 518060, China

b Univ Rennes, CNRS, ISCR (Istitut des Sciences Chimiques de Rennes) UMR 6226, Rennes, F-35000, France

c School of Machinery and Automation, Weifang University, Weifang 261061, China

[*] Corresponding authors E-mail: zhengzh@szu.edu.cn

Abstract Flexible thin-film generators are a great promising energy source for wearable device applications. In this work, Al-doped Cu_2Se thin film with highly (0*l*0) preferred orientation was achieved by magnetron co-sputtering deposition. It possessed a high *ZT* value of 0.76 at 275 °C, and further surface organic component coating treatment resulted in its exceptional flexibility. The Al dopant was proven to be successfully introduced into the lattice of Cu_2Se samples, which can decrease carrier concentration and result in the enhancement of Seebeck coefficient. Meanwhile, a significant decline in lattice thermal conductivity was achieved after Al doping. The organic component coating can prevent the fracture of inorganic thin films after bending. The resistance difference ($\Delta R/R_0$) after 1000 cycles of bending was lower than 10%, which is a great improvement compared with that in pristine thin film (over 15%). The thermoelectric device prepared by the Al-doped Cu_2Se obtained a stable power density of ~5.7 W m^{-2} at a temperature difference of 20 °C.

Graphical abstract

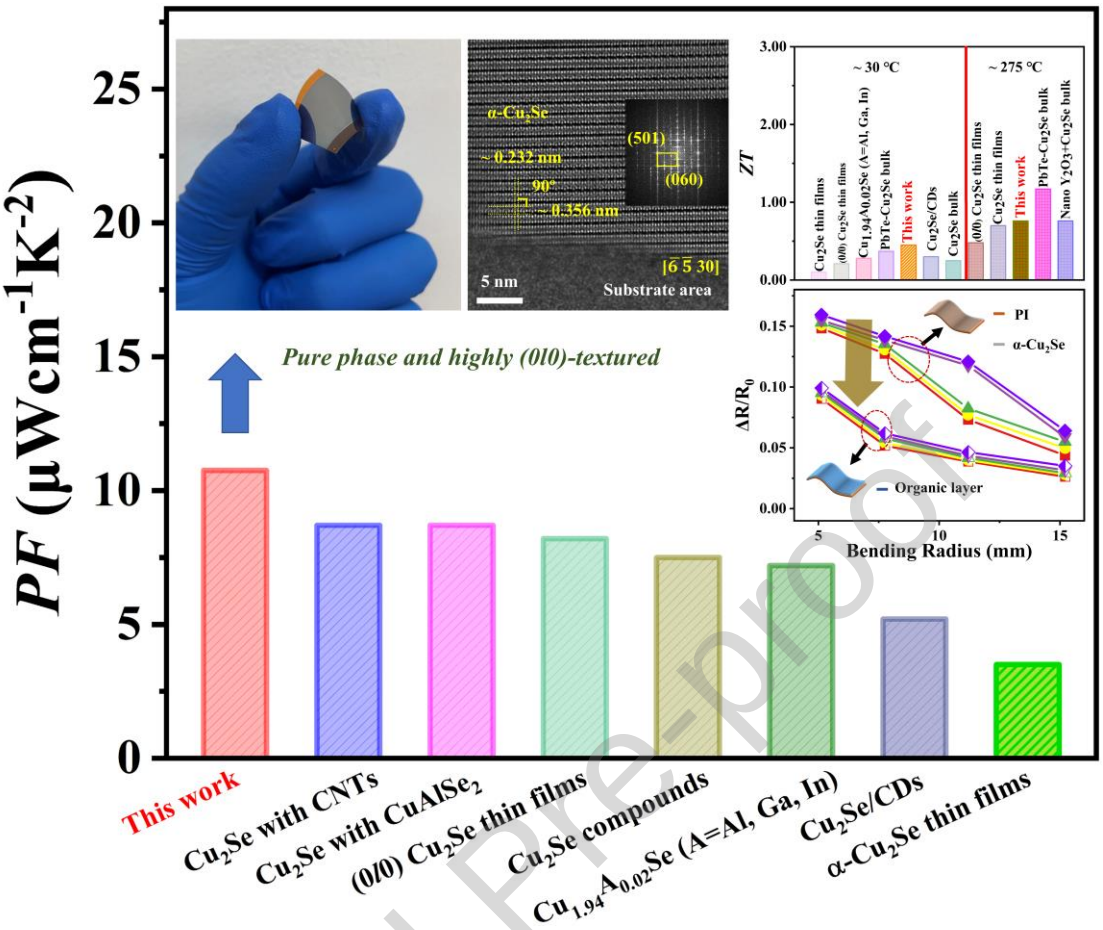

Keywords: Thermoelectric, flexibility, aluminum doped cuprous selenide, thermoelectric properties

1. Introduction

The utilization of thermoelectric (TE) properties of semiconductors is important in improving energy efficiency because it can directly convert thermal energy to electrical energy. The TE performance of materials is determined as a dimensionless figure-of-merit *ZT* ($ZT = S^2\sigma T/\kappa$, where S, σ, T, and κ are the Seebeck coefficient, electrical conductivity, absolute temperature, and thermal conductivity) [1-5]. In general, high power factor ($PF = S^2\sigma$) and low κ are required simultaneously to achieve a high *ZT* value [6-8]. In recent years, with the accelerating development of mobile and wearable electronics, promising TE devices are considerably in demand to replace traditional chemical batteries for realizing self-powered applications. Excellent flexibility and superior TE property are required at the same time to manufacture such nanoscopic TE

devices [9-12].

Organic compounds generally exhibit excellent flexibility but poorer TE properties than inorganic materials. On the contrary, the flexibility of organic thin films is always poorer than that of inorganic ones [13]. Since the investigation of mechanisms and the development of synthesis methods in the past years, inorganic TE bulk and thin film materials have received numerous expectations from researchers [14-24]. Zhang et al. [20] successfully synthesized $(Sn_{0.6}Sb_{0.4}Te)_{0.7}(Ge_{0.5}Mn_{0.5}Te)_{0.3}$ TE materials and achieved a *ZT* of over 1.5 by optimizing the carrier concentration. A peak *ZT* of 2.1 in a 2D structure design of $BiBi_2X_3$ (X = S/Se/Te) material was reported by Zhang et al. [21]. Jiang et al. [22] efficiently controlled the defect structures in GeTe and enhanced the *ZT* to be over 2.3 at 648 K. In addition, researchers focused on liquid-like inorganic TE materials, including Cu_2(S, Se, Te) and Ag_2(S, Se, Te), owing to the intrinsic mobility of Cu^+ and Ag^+ ions at high temperatures, leading to an ultrahigh *ZT* of over 2 [25-29]. Among them, p-type Cu_2Se, which possesses many advantages, such as extensive amount of raw materials, low cost, and no toxicity, has been thoroughly studied in recent decades. In accordance with the phase diagram, Cu_2Se has two types of crystal structures at different temperatures: α-phase monoclinic at temperatures below 396 K and β-phase cubic at temperatures above 396 K [30]. The phonon-liquid behavior, which can lead to ultralow thermal conductivity and maintain high electrical conductivity, originates from the mobility of Cu ions at high temperatures [31, 32]. Although Cu_2Se-based materials have a record *ZT* of ~2.6 [33], the insufficient stability, composition deviation, and low output performance of electricity generation restrict their improvement [34, 35]. Yang et al. [36] successfully introduced BiCuSeO nanoparticles into the Cu_2Se host matrix to inhibit the movement of Cu and improve the stability of the Cu_2Se. Lei et al. [37] achieved a superionic conductor behavior in Cu_2Se by dispersing SiC, which can greatly enhance electrical conductivity. Zhao et al. [38] reduced the Cu vacancy by tuning the Cu content, confirming the importance of excess Cu on the stability of α Cu_2Se, and obtained a high *ZT* of 1.44 at 873 K. Due to the excellent TE performance of Cu_2Se bulk materials, their thin films have also been extensively investigated [39-43]. Wang et al. [39] prepared Cu_2Se thin films with a *ZT* of 0.58 at 580 K

by pulsed laser deposition. Jaime et al. [40] fabricated Cu_2Se thin films through pulsed hybrid reactive magnetron sputtering and achieved a *ZT* of 0.5 at 300 K. Zhaoyang Lin et al. [41] achieved a high *PF* of ~0.46 $mWm^{-1}K^{-2}$ at 664 K in Cu_2Se thin films by spin coating. Shunya Sakane et al. [42] remarkably improved the performance of PEDOT: PSS by Cu_2Se nanowires synthesized via photoreduction. Li et al. [43] controlled the growth temperature and elemental composition of flexible Cu_2Se thin films and obtained a high *PF* of 1.92 $\mu Wcm^{-1}K^{-2}$.

In our previous work, magnetron sputtering method was performed to fabricate *α*-Cu_2Se thin films, and the carrier transport behavior was adjusted by introducing annealing, resulting a maximum power factor of 9.23 $\mu Wcm^{-1}K^{-2}$ at near room temperature [44-46]. However, the fabricated Cu_2Se-based thin films consistently had a high carrier concentration (~ 10^{21} cm^{-3}). Al is one of the highest valence metals which can more effectively reduce the carrier concentration of p-type Cu_2Se thin films than other elements with low valence. Additionally, Al doped Cu_2Se is not easy to form clusters, and can also achieve a similar preparation process and physical properties comparing to Cu. These significant properties allow Al to achieve a precise and controllable doping in Cu_2Se thin films. In this work, Al was selected as dopant and the results show that the *PF* of Cu_2Se thin film was enhanced to 10.75 $\mu Wcm^{-1}K^{-2}$ at 30 °C due to the improvement of Seebeck coefficient after Al doping. Meanwhile, all the synthesized thin films have low thermal conductivity, resulting in high *ZT* values of 0.76 at 275 °C, as shown in Figs. 1a and 1b. These findings are comparable to those of recent studies. Meanwhile, polyvinyl laurate organic photoresist was used to protect the Cu_2Se thin film for the first time, and resulted in the $\Delta R/R_0$ lower than 10% after 1000 cycles of bending at a radius of 5 mm. This factor is a great improvement compared with that in pristine thin film (~15%), indicating the outstanding flexibility of the as-synthesized Al-doped α-Cu_2Se thin films. The improved mechanical property of Cu_2Se thin film is due to the natural flexibility of organic components and the good adhesion between photoresist and inorganic film. Eventually, the Cu_2Se-based TE generator with 10 legs connected by Ag/Mo electrode can achieve a maximum power density of ~5.7 Wm^{-2} at a 20 °C temperature gradient.

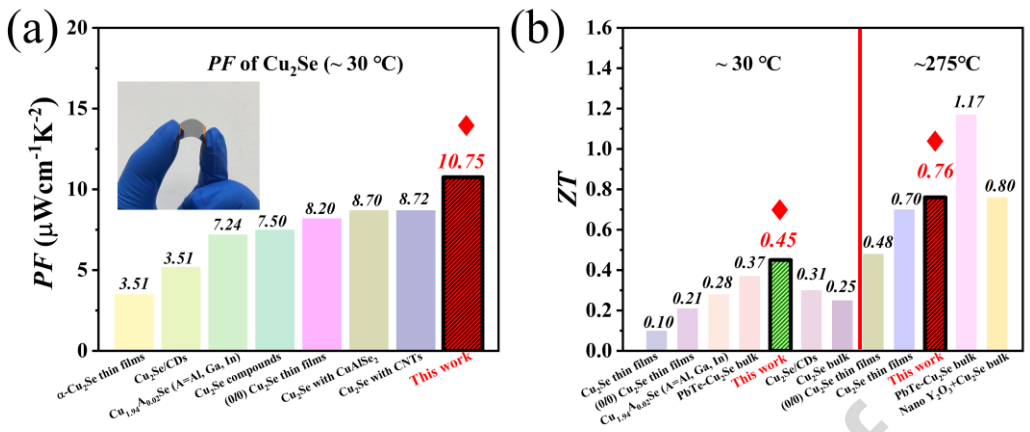

Fig. 1. (a) Comparison of the highest power factor at 30 °C with other literature; (b) comparison of the highest *ZT* values at 30 °C and at 275 °C with other literature (*PF* (30 °C) [8], [26], [27], [28], [29] ,[44], [46]; *ZT* (30 °C) [7], [26], [27], [31], [39], [46]; *ZT* (275 °C) [7], [32], [39], [46].).

2. Experimental Section

Cu_2Se-based thin films with different Al contents (from 1.6 at.% to 5.2 at.%) were prepared via magnetron co-sputtering method as shown in Fig. S1 (Supporting Information). First, polyimide (PI) substrates were washed by detergent, ultrapure water, and ethanol one after another for several times and then dried in a heat box at 40 °C. The sputtering targets were Cu (99.9%), Cu_2Se (99.9%), and Al (99.9%). During the sputtering process, the vacuum system was first kept to 8×10^{-4} Pa, and the working pressure was 0.5 Pa. The argon flow was maintained during the whole magnetron sputtering process. The sputtering power of Cu_2Se, Cu, and Al targets were fixed at 55 W, 15 W, and 10 W, respectively. After deposition, the as-deposited thin films were annealed under nitrogen atmosphere at 300 °C for 30 min. Cu_2Se-based single-leg generators were fabricated using the synthesized Cu_2Se thin films with an external mask. The geometry of TE legs was fixed at 26 mm × 2 mm, the electrode was made by Ag/Mo, and 10 TE legs were fabricated on a PI substrate. An organic coating material (polyvinyl laurate) was used to improve the flexibility of the as-fabricated TE generator. First, the Cu_2Se thin films were fixed and flatted on a glass. Second, an appropriate amount of polyvinyl laurate was dropped on the thin films after vacuum. The thin films were placed in a centrifuge for 10 s with a rotation speed of 2000 r/s to homogenize the

organic layer. Then, the samples were heated at 95 °C for 2 min and exposed to ultraviolet light for 15 s.

The crystal structures of the synthesized samples were measured by X-ray diffraction (XRD, D/max 2500 Rigaku Corporation) with 2θ range from 10º to 60º. Scanning electron microscope (SEM, Zeiss Supra55) was utilized for microstructure analysis. Nanostructure observation was carried out by transmission electron microscopy (TEM, JEM3200FS). The composition content was detected by energy-dispersive X-ray spectroscopy (EDS, Bruker Quantax 200). An X-ray photoelectron spectroscopy (XPS, Thermo Escalab 250XI) was employed to investigate the chemical states of all specimens, and all samples were etched for 30 s before the measurement. The Van der Pauw Hall measurement system (HL5500PC, Nano metrics) was used to characterize the carrier concentration and mobility. The temperature-dependent Seebeck coefficient and electrical conductivity were characterized by SBA458. The errors of the evaluated data were determined as 5% for S, 5% for σ, and 10% for $S^2\sigma$. Thermal conductivity was measured by the 3ω method with a Cu_2Se thin film deposited on a Van -der -Pauw chip through a thin film comprehensive physical property analyzer (TFA-LINSES) [47, 48]. The electronic energy band was calculated by the first-principles plane-wave pseudopotential formalism in the VASP package (Supporting Information).

3. Results and Discussion

The EDS results are shown in Table S1 (Supporting Information). They indicated that the Cu/Se ratios of all the synthesized specimens are relatively similar to the stoichiometric ratio of Cu_2Se but rich in Cu. Fig. 2a displays the XRD results and shows the high crystallinity of all the Cu_2Se-based thin films. All the synthesized samples have two main diffraction peaks related to the crystal planes (030) and (060), corresponding to the α-Cu_2Se crystal structure (PDF #47-1448). The main diffraction angles of the un-doped sample are located at 13.02° and 26.18°. With the increase in Al content, the diffraction peaks gradually shifted, indicating that Al was successfully introduced into the lattice. Meanwhile, the intensities of diffraction peaks are very high, indicating the preferred orientation in the as-deposited Cu_2Se thin films. Hence, the orientation factor was calculated [44], and the orientation factors are listed in Fig. 2c for comparison. The

orientation factors improved to over 0.9, indicating an enhancement of the oriented growth by Al doping. XPS was performed to further evaluate the chemical status of the Al-doped Cu_2Se samples, as shown in Figs. 2d -2f. Fig. 2d shows the Cu curves, and the main peaks are related to Cu $2p_{1/2}$ and Cu $2p_{3/2}$ orbits [44, 49]. The Se curves can be identified into two symmetric peaks, which are related to Se $3d_{5/2}$ and Se $3d_{3/2}$ orbits, from a broad peak ranging from 52 eV to 57 eV [49]. Fig. 2f demonstrates the Al curves. The intensity of binding energy on the Al 2p orbit is much lower than that on the Cu $3p_{1/2}$ and $3p_{3/2}$ orbits due to the rich Cu and the poor Al. No obvious shifts in the Al 2p peaks can be observed, corresponding to the Al^{3+} chemical state, among different Al-doped samples.

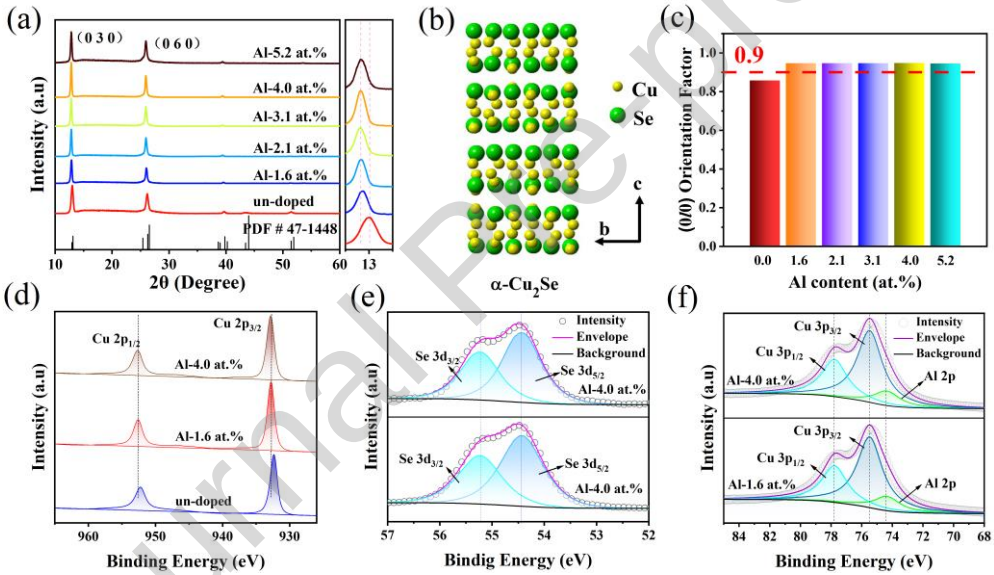

Fig. 2. (a) X-ray diffraction (XRD) patterns of Cu_2Se-based thin films with different Al contents; (b) crystal structure of α-Cu_2Se material; (c) calculated orientation factors based on XRD results; (d) Cu 2p, (e) Se 3d, and (f) Al 2p X-ray photoelectron spectroscopy (XPS) for as-synthesized samples of un-doped, Al-1.6 at.%, and Al-4.0 at.%.

Scanning electron microscope and spherical aberration-corrected scanning transmission electron microscopy (Cs-STEM) were performed. The micro surface of the as-deposited Cu_2Se is smooth, as shown in Fig. S2 (Supporting Information). No obvious agglomeration can be found after Al doping. Fig. 3a shows the full cross-sectional view of Cu_2Se (Al-4.0 at.%) and the thickness of the specimen is ~500 nm.

Fig. 3b shows a high-angle annular dark field (HAADF) image of the yellow square in Fig. 3a. The grain boundaries can be observed in the dark region (Fig. S3, Supporting Information). The EDS maps of Se, Cu, and Al in Fig. 3b suggest the uniform distribution of these elements. Fig. 3c depicts an HRTEM image of the Cu_2Se thin film and shows a well-adherent and smooth connection between the thin film and substrate interface. The inset of Fig. 3c is an FFT image of the HRTEM figure. Diffraction spots related to (060) and (501) planes can be identified. Fig. 3d shows the lattice strains of the red square in Fig. 3c along different directions. Obvious strain fields between layers can be found, which can be estimated by the introduction of Al-doping. Fig. 3e and Fig. S4(a) (Supporting Information) demonstrate the crystal structure of α-Cu_2Se. The lattice framework was formed by Se atoms, which have a brighter view due to a higher atomic number of Se comparing to that of Cu and Al, and a similar result was observed by Li et al [50]. After Al doping, some host atoms are found in the crystalline domain, as shown in Fig. 3f and Fig. S4(b) (Supporting Information), and the Se atoms without undergoing a significant rearrangement (Fig. S4(c), Supporting Information). This result can support that Al was involved into the lattice of Cu_2Se, which also matches the results of XRD (Fig. 2(a)). To further confirm the conclusion above, formation energy calculations were carried out based on DFT simulation. The results indicate that the formation energy of interstitial Al defect is -2.835 eV and substitution Al is -2.587 eV under the Cu-rich condition. Therefore, similar formation energy indicates that both of interstitial Al defect and substitution Al defect are forming Cu_2Se defects and play dominant roles in α-Cu_2Se.

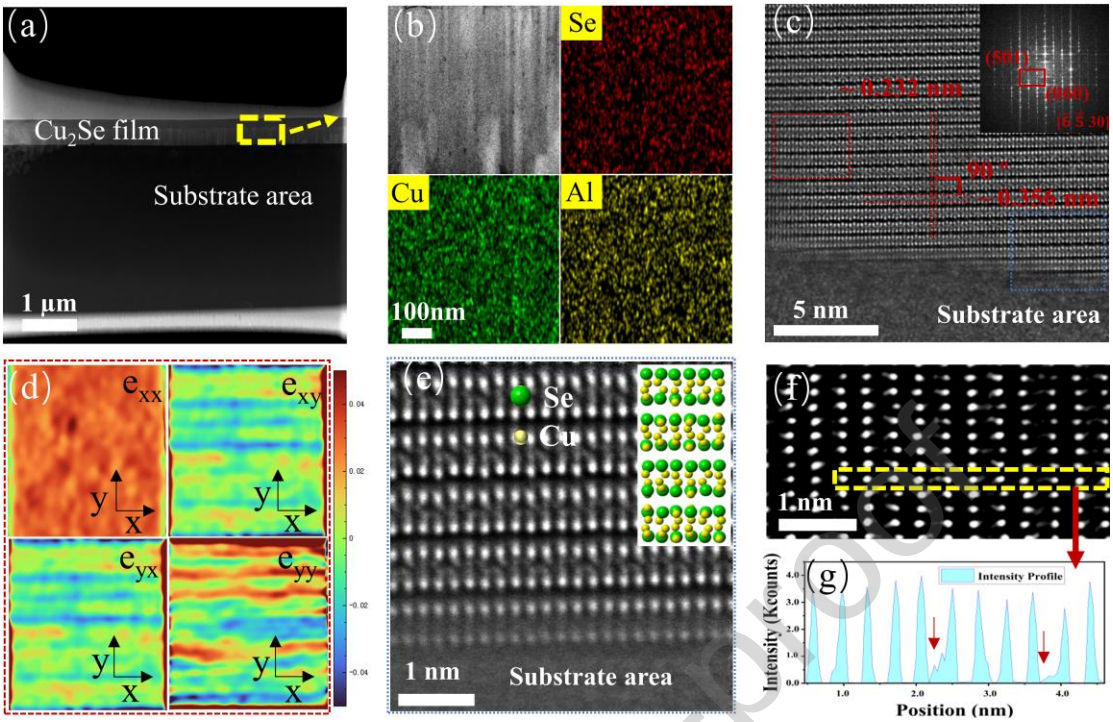

Fig. 3. (a) Full cross-sectional image of Cu_2Se thin film with 4.0 at.% Al content under spherical aberration-corrected scanning transmission electron microscopy; (b) high-angle annular dark-field image of Cu_2Se corresponding to the yellow square (a) and element distribution map of Se, Cu, and Al; (c) high-resolution TEM image of Cu_2Se thin film next to substrate area with a fast Fourier transform; (d) lattice strains of the red square in (c) along different directions; (e) crystal structure of α-Cu_2Se of the blue square in (c); (f) adjusted image from (e); (g) intensity line profiles of (f).

Fig. 4a shows the Seebeck coefficient (S) of the synthesized Cu_2Se thin films as a function of temperature. The positive values suggest that the synthesized Cu_2Se thin films are all p-type semiconductors. The S first decreases with the increase in temperature and then increases when the temperature reaches over 150 °C, suggesting a typical transition of phase in Cu_2Se thin films [25, 29]. After Al doping, the S of the synthesized samples gradually increases, and the Al-5.2 at.% sample has the highest S values of 163.2 μV K^{-1} at 30 °C and 258.7 μV K^{-1} at 300 °C. This S value is an improvement of around three times compared with that of the pristine sample due to the optimized effective mass and carrier concentration (Fig. 4d). Meanwhile, Fig. 4b shows the electrical conductivity (σ) of the as-deposited thin films. The increase in temperature leads to a decrease in electrical conductivity. This phenomenon is

common in Cu_2Se-based TE materials [8, 35, 36]. The carrier concentration (n) and mobility (μ) are shown in Fig. 4c. The μ increases from 11.2 $cm^2 V^{-1} s^{-1}$ to 68.6 $cm^2 V^{-1} s^{-1}$ with increasing Al content, and the n of all samples decreases from 1.08×10^{21} cm^{-3} to 9.02×10^{19} cm^{-3} due to the existence of trivalent Al^{3+}, which is also confirmed in Fig. 2f. The carrier concentration and mobility can further confirm the improvement of S and σ. Thus, Al doping can satisfactorily adjust the transport behavior of Cu_2Se. The improvement in S can be described as follows:

$$S = \frac{8\pi^2 k_B^2 T}{3e\hbar^2}\, m^* \left(\frac{\pi}{3n}\right)^{2/3}, \tag{1}$$

where k_B, e, $\hbar$, and m^* are Boltzmann's constant, the charge of the electron, Planck's constant, and the density of states' effective mass, respectively. The theory S and m^* are calculated from the single parabolic band mode, as follows [51]:

$$S(\eta) = \frac{k_B}{e}\cdot\left[\frac{\left(r+\frac{5}{2}\right).F_{r+\frac{3}{2}}(\eta)}{\left(r+\frac{3}{2}\right).F_{r+\frac{1}{2}}(\eta)} - \eta\right], \tag{2}$$

$$n_H = \frac{1}{e.R_H} = \frac{(2m^*.k_BT)^{\frac{3}{2}}}{3\pi^2\hbar^3}\cdot\frac{\left(r+\frac{3}{2}\right)^2.F_{r+\frac{1}{2}^2}(\eta)}{\left(2r+\frac{3}{2}\right).F_{2r+\frac{1}{2}}(\eta)}, \tag{3}$$

$$\mu_H = \left[\frac{e\pi\hbar^4}{\sqrt{2}(k_BT)^{\frac{3}{2}}}\frac{C_1}{E_{def}^2(m^*)^{\frac{5}{2}}}\right]\frac{\left(2r+\frac{3}{2}\right).F_{2r+\frac{1}{2}}(\eta)}{\left(r+\frac{3}{2}\right)^2.F_{r+\frac{1}{2}}(\eta)}, \tag{4}$$

$$F_j(\eta_F) = \int_0^\infty \frac{x^j}{1+e^{x-\eta_F}}\,dx, \tag{5}$$

where j is the Fermi integral of order, η_F and $\hbar$ are reduced Fermi level (E_f/k_BT) and Plank constant. By using the experimentally measured S and n in the above formula and assuming acoustic phonon scattering is prominent (i.e. r = -1/2) [52], the Pisarenko relationship at room temperature was calculated (Fig. 4d). This is because the increase of effective mass under similar carrier concentration after Al doping will lead to an increase in S. The energy band of Cu_2Se and $Cu_{1.98}Al_{0.02}Se$ are shown in Figs. 4e and 4f. The Fermi level slightly shifts to the conduction band after Al doping, indicating the decrease in the hole concentration and thus resulting in reducing σ, which matches the

theoretical hypothesis as well. Fig. 4g plots the *PF* as a function of temperature and shows that Al -doping can significantly improve the *PF* value of the Al-1.6 at.% sample near room temperature compared with that of the pristine Cu_2Se, which is as high as 10.75 μW cm^{-1} K^{-2} at 30 °C. Fig. 4h shows the measured total thermal conductivities of Cu_2Se thin films revealing a decreasing trend with the increase in Al content. The lattice thermal conductivities are also lower after Al doping than those in the pristine sample (Fig. S5, Supporting Information). This phenomenon may be caused by the scattering effect of defects and intrinsic preferred orientation in Cu_2Se thin films (Fig. 3). Meanwhile, the *ZT* values were calculated, as shown in Fig. 4i. The Al-doped samples exhibit significantly enhancement in *ZT* values compared with the pristine Cu_2Se thin film due to the significant decrease in thermal conductivity. Remarkable *ZT* values of ~0.45 at 30 °C and ~0.76 at 275 °C were achieved in the Al-4.0 at.% sample.

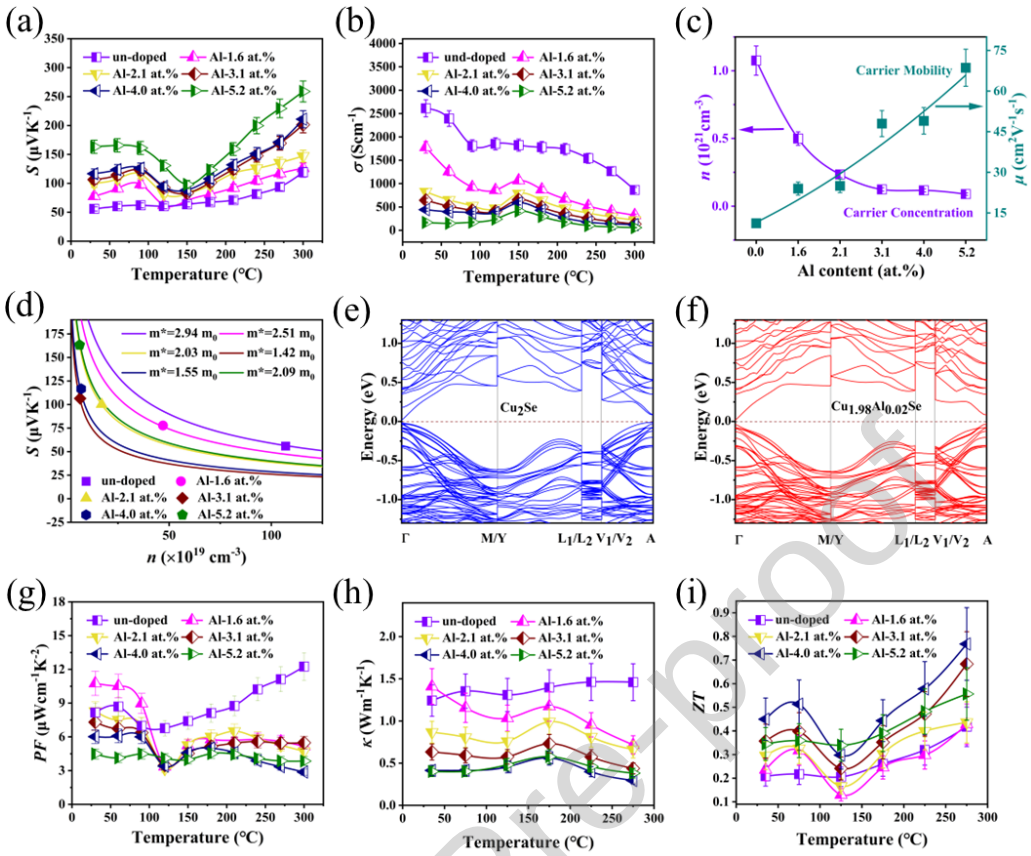

Fig. 4. Temperature-dependent TE properties of Cu_2Se films with various Al contents: (a) Seebeck coefficient; (b) electrical conductivity; (c) carrier concentration and mobility as a function of Al content; (d) calculated Seebeck coefficient curves as a function of carrier concentration; energy band structure of (e) pristine Cu_2Se thin film and (f) Al-doped Cu_2Se thin film; (g) temperature-dependent power factor of as-deposited Al-doped Cu_2Se; (h) temperature-dependent thermal conductivity of as-synthesized Al-doped Cu_2Se; (i) temperature-dependent *ZT* of as-synthesized Al-doped Cu_2Se films.

The flexibility of Cu_2Se-based thin films was further investigated, as shown in Fig.5a. The $\Delta R/R_0$ of the as-fabricated Cu_2Se thin films without an organic coating layer. The $\Delta R/R_0$ sharply increases up to 15% with the decrease in bending radius from 20 mm to 5 mm under different bending cycles from 200 to 1000. In addition, the micro surface (Fig. S6, Supporting Information) reveals that the films were severely damaged after bending. An organic coating material (polyvinyl laurate) was employed on the Cu_2Se thin films by spin coating to solve this problem, as shown in Fig. 5b. With a ~5.0 μm-thick organic coating layer, the flexibility of Cu_2Se thin films significantly

improved, and the $\Delta R/R_0$ of all samples is lower than 10% (Fig. 5c). The morphologies before and after bending are shown in Fig. S6 (Supporting Information). The results suggest that the flexibility was improved by the absence of fracture after bending. Fig. 5d shows the output I-V and output power of the generator with 10 legs. The photo of the fabricated generator is shown as an inset image of Fig. 5d. The output electricity properties gradually increase with the increase in temperature difference, and a maximum power of ~110 nW was achieved at a temperature difference of 20 °C. The calculated power density is ~5.7 Wm^{-2}, as shown in Fig. 5e. Meanwhile, the output power of the as-fabricated device after bending is plotted in Fig. 5f. The output properties of the device with an organic coating layer can be maintained compared with those of the device without an organic layer. The above analysis shows that a feasible solution was successfully performed to improve the flexibility of Cu_2Se thin films.

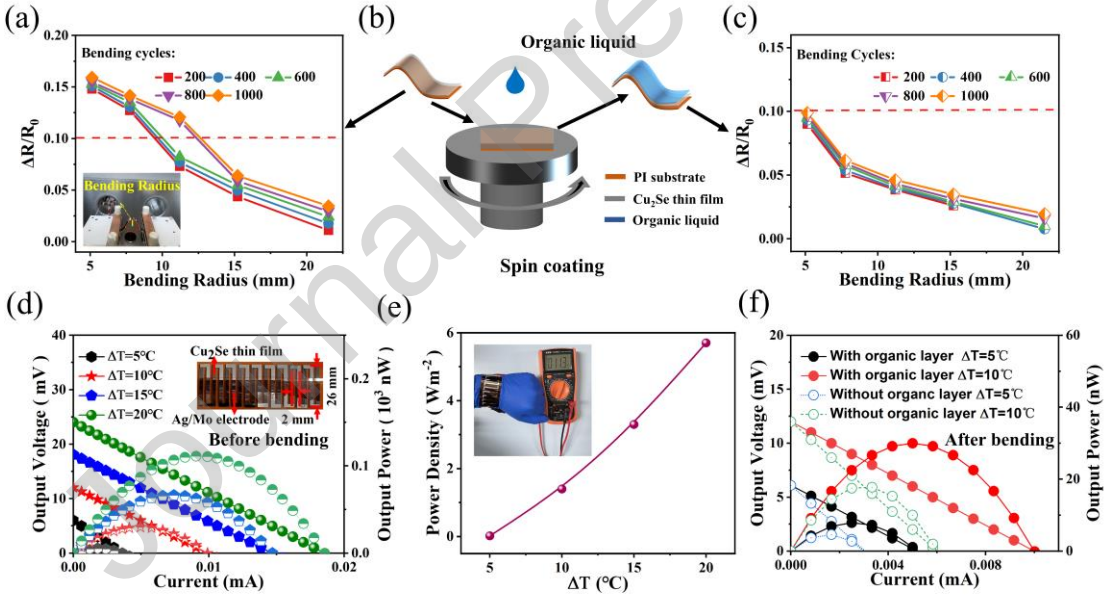

Fig. 5. (a) Resistance difference ($\Delta R/R_0$) of flexible Cu_2Se-based thin films without an organic component coating layer; (b) illustration of spin-coating process of an organic coating layer onto Cu_2Se-based thin films; (c) $\Delta R/R_0$ of flexible Cu_2Se-based thin films with an organic coating layer; (d) output I-V and calculated output power curves before bending; (e) calculated power density; (f) output power of the as-fabricated generator after bending.

4. Conclusion

In this work, Al doping and organic coating strategies were successfully performed to further improve the TE properties and flexibility of p-type Cu_2Se thin films. Flexible Cu_2Se-based thin films were fabricated, and the *S* value increased from 57.2 μV K^{-1} to 163.2 μV K^{-1} after Al doping. The Al-doped samples have low thermal conductivity and high *ZT* values of 0.45 at 30 °C and 0.76 at 275 °C. Moreover, the flexibility of Cu_2Se thin films was significantly improved by using an organic layer coating. The as-fabricated flexible generator achieved a remarkable output power of ~110 nW, and the power density is ~5.7 Wm^{-2} at a temperature difference of 20 °C. This study provides convenient and efficient strategies to improve the TE performance and flexibility of Cu_2Se thin films and devices.

Acknowledgements

This work was supported by the National Natural Science Foundation of China (No. 62274112), Guangdong Basic and Applied Basic Research Foundation (2022A1515010929), and Science and Technology plan project of Shenzhen (JCYJ20220531103601003). The authors are thankful for the assistance on HAADF-STEM observation received from the Electron Microscope Center of Shenzhen University.

References

[1] J.L. Blackburn, A.J. Ferguson, C. Cho, J.C. Grunlan, Carbon-Nanotube-Based Thermoelectric Materials and Devices, Adv. Mater., 30 (2018) 35.

[2] Z.G. Chen, X.L. Shi, L.D. Zhao, J. Zou, High-performance SnSe thermoelectric materials: Progress and future challenge, Prog. Mater. Sci., 97 (2018) 283-346.

[3] L. Yang, Z.G. Chen, M.S. Dargusch, J. Zou, High Performance Thermoelectric Materials: Progress and Their Applications, Advanced Energy Materials, 8 (2018) 28.

[4] X.Y. Zhou, Y.C. Yan, X. Lu, H.T. Zhu, X.D. Han, G. Chen, Z.F. Ren, Routes for high-performance thermoelectric materials, Mater. Today, 21 (2018) 974-988.

[5] T.J. Zhu, C.G. Fu, H.H. Xie, Y.T. Liu, X.B. Zhao, High Efficiency Half-Heusler Thermoelectric Materials for Energy Harvesting, Advanced Energy Materials, 5 (2015) 13.

[6] H. Bai, X. Su, D. Yang, Q. Zhang, G. Tan, C. Uher, X. Tang, J. Wu, An Instant Change of Elastic Lattice Strain during Cu_2Se Phase Transition: Origin of Abnormal Thermoelectric Properties,

Advanced Functional Materials, 31 (2021) 7.

[7] M. Wu, H.H. Cui, S. Cai, S. Hao, Y. Liu, T.P. Bailey, Y. Zhang, Z. Chen, Y. Luo, C. Uher, C. Wolverton, V.P. Dravid, Y. Yu, Z.Z. Luo, Z. Zou, Q. Yan, M.G. Kanatzidis, Weak Electron–Phonon Coupling and Enhanced Thermoelectric Performance in n-type PbTe–Cu_2Se via Dynamic Phase Conversion, Advanced Energy Materials, 13 (2022) 9.

[8] J. Zhang, C. Zhang, T. Zhu, Y. Yan, X. Su, X. Tang, Mechanical Properties and Thermal Stability of the High-Thermoelectric-Performance Cu_2Se Compound, ACS Appl Mater Interfaces, 13 (2021) 45736-45743.

[9] Z.H. Zheng, X.L. Shi, D.W. Ao, W.D. Liu, Y.X. Chen, F. Li, S. Chen, X.Q. Tian, X.R. Li, J.Y. Duan, H.L. Ma, X.H. Zhang, G.X. Liang, P. Fan, Z.G. Chen, Rational band engineering and structural manipulations inducing high thermoelectric performance in n-type $CoSb_3$ thin films, Nano Energy, 81 (2021) 21.

[10] Y. Wang, L. Yang, X.L. Shi, X. Shi, L.D. Chen, M.S. Dargusch, J. Zou, Z.G. Chen, Flexible Thermoelectric Materials and Generators: Challenges and Innovations, Adv. Mater., 31 (2019) 47.

[11] C. Gayner, Y. Amouyal, Energy Filtering of Charge Carriers: Current Trends, Challenges, and Prospects for Thermoelectric Materials, Advanced Functional Materials, 30 (2020) 17.

[12] D.L. Li, Y.N. Gong, Y.X. Chen, J.M. Lin, Q. Khan, Y.P. Zhang, Y. Li, H. Zhang, H.P. Xie, Recent Progress of Two-Dimensional Thermoelectric Materials, Nano-Micro Lett., 12 (2020) 40.

[13] Badgujar. K. C, Bhanage. B. M, Immobilization of lipase on biocompatible co-polymer of polyvinyl alcohol and chitosan for synthesis of laurate compounds in supercritical carbon dioxide using response surface methodology, Process Biochemistry, 50 (2015) 1224-1236.

[14] N. Nandihalli, C.J. Liu, T. Mori, Polymer based thermoelectric nanocomposite materials and devices: Fabrication and characteristics, Nano Energy, 78 (2020) 29.

[15] X.L. Shi, J. Zou, Z.G. Chen, Advanced Thermoelectric Design: From Materials and Structures to Devices, Chem. Rev., 120 (2020) 7399-7515.

[16] Y.H. Jia, Q.L. Jiang, H.D. Sun, P.P. Liu, D.H. Hu, Y.Z. Pei, W.S. Liu, X. Crispin, S. Fabiano, Y.G. Ma, Y. Cao, Wearable Thermoelectric Materials and Devices for Self-Powered Electronic Systems, Adv. Mater., 33 (2021) 46.

[17] J. Mao, G. Chen, Z.F. Ren, Thermoelectric cooling materials, Nat. Mater., 20 (2021) 454-461.

[18] S.D. Xu, X.L. Shi, M. Dargusch, C.A. Di, J. Zou, Z.G. Chen, Conducting polymer-based

flexible thermoelectric materials and devices: From mechanisms to applications, Prog. Mater. Sci., 121 (2021) 66.

[19] L. Zhang, X.L. Shi, Y.L. Yang, Z.G. Chen, Flexible thermoelectric materials and devices: From materials to applications, Mater. Today, 46 (2021) 62-108.

[20] Q. Zhang, R.Y. Wang, K. Song, X.J. Tan, H.Y. Hu, Z. Guo, G. Wu, P. Sun, G.Q. Liu, J. Jiang, Raised solubility in SnTe by $GeMnTe_2$ alloying enables converged valence bands, low thermal conductivity, and high thermoelectric performance, Nano Energy, 94 (2022) 10.

[21] X.W. Zhang, Y. Guo, Z.B. Zhou, Y.H. Li, Y.F. Chen, J.L. Wang, A general strategy for designing two-dimensional high-efficiency layered thermoelectric materials, Energy & Environmental Science, 14 (2021) 4059-4066.

[22] Y.L. Jiang, J.F. Dong, H.L. Zhuang, J.C. Yu, B. Su, H.Z. Li, J. Pei, F.H. Sun, M. Zhou, H.H. Hu, J.W. Li, Z.R. Han, B.P. Zhang, T.K. Mori, J.F. Li, Evolution of defect structures leading to high ZT in GeTe-based thermoelectric materials, Nat. Commun., 13 (2022) 9.

[23] T. Ishibe, Y. Komatsubara, K. Ishikawa, S. Takigawa, N. Naruse, Y. Mera, Y. Yamashita, Y. Ohishi, Y. Nakamura, Boosting thermoelectric performance in epitaxial GeTe film/Si by domain engineering and point defect control, ACS Appl. Mater. Interfaces, 15 (2023) 26104.

[24] F. Robinson, V. Sethi, C.H.K. De Groot, A.L. Hector, R.M. Huang, G. Reid, Low-Pressure CVD of GeE (E = Te, Se, S) Thin Films from Alkylgermanium Chalcogenolate Precursors and Effect of Deposition Temperature on the Thermoelectric Performance of GeTe, ACS Appl. Mater. Interfaces, 13 (2021) 47773-47783.

[25] W. Cao, Z. Wang, L. Miao, J. Shi, R. Xiong, Thermoelectric Properties of Strained beta-Cu_2Se, ACS Appl Mater Interfaces, 13 (2021) 34367-34373.

[26] Q. Hu, Y. Zhang, Y. Zhang, X.-J. Li, H. Song, High thermoelectric performance in Cu_2Se/CDs hybrid materials, Journal of Alloys and Compounds, 813 (2020) 6.

[27] J.H. Kim, S. Oh, W.H. Sohn, J.-S. Rhyee, S.-D. Park, H. Kang, D. Ahn, Thermoelectric, thermodynamic, and structural properties in $Cu_{1.94}A_{0.02}Se$ (A= Al, Ga, and In) polycrystalline compounds, Acta Materialia, 100 (2015) 32-38.

[28] R. Lu, T.P. Bailey, C. Uher, P.F.P. Poudeu, Ultrafine Interwoven Dendritic $Cu_2Se/CuFeSe_2$ Composites with Enhanced Thermoelectric Performance, ACS Applied Energy Materials, 3 (2020) 9133-9142.

[29] R. Nunna, P. Qiu, M. Yin, H. Chen, R. Hanus, Q. Song, T. Zhang, M.-Y. Chou, M.T. Agne, J. He, G.J. Snyder, X. Shi, L. Chen, Ultrahigh thermoelectric performance in Cu_2Se-based hybrid materials with highly dispersed molecular CNTs, Energy & Environmental Science, 10 (2017) 1928-1935.

[30] W.D. Liu, L. Yang, Z.G. Chen, Cu_2Se thermoelectrics: property, methodology, and device, Nano Today, 35 (2020) 24.

[31] L. Bo, R. Zhang, H. Zhao, Y. Hou, X. Wang, J. Zhu, L. Zhao, M. Zuo, D. Zhao, Achieving High Thermoelectric Properties of Cu_2Se via Lattice Softening and Phonon Scattering Mechanism, ACS Applied Energy Materials, 5 (2022) 6453-6461.

[32] R. Ma, D. Yang, X. Li, H. Song, Y. Zhang, Thermoelectric properties in nano Y_2O_3 dispersed Cu_2Se, Applied Physics A, 128 (2022) 6.

[33] A.A. Olvera, N.A. Moroz, P. Sahoo, P. Ren, T.P. Bailey, A.A. Page, C. Uher, P.F.P. Poudeu, Partial indium solubility induces chemical stability and colossal thermoelectric figure of merit in Cu_2Se, Energy & Environmental Science, 10 (2017) 1668-1676.

[34] S. Islam, M. Li, U. Aydemir, X. Shi, L.D. Chen, G.J. Snyder, X.L. Wang, Giant enhancement of the figure-of-merit over a broad temperature range in nano-boron incorporated Cu_2Se, J. Mater. Chem. A, 6 (2018) 18409-18416.

[35] Z. Zhang, K. Zhao, T.-R. Wei, P. Qiu, L. Chen, X. Shi, Cu_2Se-Based liquid-like thermoelectric materials: looking back and stepping forward, Energy & Environmental Science, 13 (2020) 3307-3329.

[36] D.W. Yang, X.L. Su, J. Li, H. Bai, S.Y. Wang, Z. Li, H. Tang, K.C. Tang, T.T. Luo, Y.G. Yan, J.S. Wu, J.H. Yang, Q.J. Zhang, C. Uher, M.G. Kanatzidis, X.F. Tang, Blocking Ion Migration Stabilizes the High Thermoelectric Performance in Cu_2Se Composites, Adv. Mater., 32 (2020) 10.

[37] J.D. Lei, Z. Ma, D. Zhang, Y.Q. Chen, C. Wang, X.Y. Yang, Z.X. Cheng, Y.X. Wang, High thermoelectric performance in Cu_2Se superionic conductor with enhanced liquid-like behaviour by dispersing SiC, J. Mater. Chem. A, 7 (2019) 7006-7014.

[38] X.D. Zhao, S.T. Ning, N. Qi, Y.H. Li, Y. Dong, H.J. Zhang, J.D. Liu, B.J. Ye, Z.Q. Chen, Synergetic Optimization of Electrical and Thermal Transport Properties by Cu Vacancies and Nanopores in Cu_2Se, ACS Appl. Mater. Interfaces, 13 (2021) 58936-58948.

[39] A. Wang, Y. Xue, J. Wang, X. Yang, J. Wang, Z. Li, S. Wang, High thermoelectric performance

of Cu_2Se-based thin films with adjustable element ratios by pulsed laser deposition, Materials Today Energy, 24 (2022) 8.

[40] J.A. Perez-Taborda, L. Vera, O. Caballero-Calero, E.O. Lopez, J.J. Romero, D.G. Stroppa, F. Briones, M. Martin-Gonzalez, Pulsed Hybrid Reactive Magnetron Sputtering for High zT Cu_2Se Thermoelectric Films, Adv. Mater. Technol., 2 (2017) 6.

[41] Z.Y. Lin, C. Hollar, J.S. Kang, A.X. Yin, Y.L. Wang, H.Y. Shiu, Y. Huang, Y.J. Hu, Y.L. Zhang, X.F. Duan, A Solution Processable High-Performance Thermoelectric Copper Selenide Thin Film, Adv. Mater., 29 (2017) 1606662.

[42] S. Sakane, S. Miwa, T. Miura, K. Munakata, T. Ishibe, Y. Nakamura, H. Tanaka, Thermoelectric Properties of PEDOT:PSS Containing Connected Copper Selenide Nanowires Synthesized by the Photoreduction Method, ACS Omega, 7 (2022) 32101.

[43] Y.L. Li, Y.M. Zhong, D.L. Zhang, J.Y. Niu, M. Nisar, M. Wei, G.X. Liang, P. Fan, Z.H. Zheng, Enhanced Thermoelectric Properties of Cu2Se Flexible Thin Films by Optimizing Growth Temperature and Elemental Composition, ACS Appl. Energ. Mater., 5 (2022) 13964-13970.

[44] P. Fan, X.l. Huang, T.b. Chen, F. Li, Y.x. Chen, B. Jabar, S. Chen, H.l. Ma, G.x. Liang, J.t. Luo, X.h. Zhang, Z.h. Zheng, α-Cu_2Se thermoelectric thin films prepared by copper sputtering into selenium precursor layers, Chemical Engineering Journal, 410 (2021) 9.

[45] X.L. Huang, D.W. Ao, T.B. Chen, Y.X. Chen, F. Li, S. Chen, G.X. Liang, X.H. Zhang, Z.H. Zheng, P. Fan, High-performance copper selenide thermoelectric thin films for flexible thermoelectric application, Materials Today Energy, 21 (2021) 8.

[46] Z.H. Zheng, D.L. Zhang, B. Jabar, T.B. Chen, M. Nisar, Y.F. Chen, F. Li, S. Chen, G.X. Liang, X.H. Zhang, P. Fan, Y.X. Chen, Realizing high thermoelectric performance in highly (0*l*0)-textured flexible Cu_2Se thin film for wearable energy harvesting, Materials Today Physics, 24 (2022) 8.

[47] Linseis, V., Volklein, F., Reith, H., Nielsch, K., Woias, P. Advanced platform for the in-plane ZT measurement of thin films. Rev. Sci. Instrum. 89 (2018) 9.

[48] Linseis, V., Volklein, F., Reith, H., Woias, P., Nielsch, K. Platform for in-plane ZT measurement and Hall coefficient determination of thin films in a temperature range from 120 K up to 450 K. Mater. Res. 31 (2016) 3196-3204.

[49] W.H. Shi, J.S. Lian, Facile synthesis of copper selenide with fluffy intersected-nanosheets decorating nanotubes structure for efficient oxygen evolution reaction, Int. J. Hydrog. Energy, 44

(2019) 22983-22990.

[50] Z.L.Li, J.X.Wang, X.Q.Yang, Flexible oriented α-Cu_2Se films and devices with remarkable power factor and output power at near-room temperature, Materials Today Physics, 31 (2023) 9.

[51] Y. Xu, W. Li, C. Wang, J. Li, Z. Chen, S. Lin, Y. Chen and Y. Pei, Performance optimization and single parabolic band behavior of thermoelectric MnTe, J. Mater. Chem. A, 5 (2017) 19143.

[52] J. Shen, Z. Chen, S. lin, L. Zheng, W. Li and Y. Pei, Single parabolic band behavior of thermoelectric p-type CuGaTe2 J. Mater. Chem. C, 4 (2016) 209.

Credit author statement

Dong Yang: Conceptualization, Data curation, Writing-Original draft preparation. **Dongliang Zhang and Dongwei Ao:** Formal analysis. **Akaash Nissar and Adil Mansoo：** Methodology. **Li Fu:** Resources. **Yuexing Chen:** Writing - review & editing. **Hongli Ma and Guangxing Liang:** Data curation. **Xianghua Zhang and Ping Fan:** Project administration. **Zhuanghao Zheng:** Supervision.

Declaration of interest statement

The authors declare that they have no known competing financial interests or personal relationships that could have appeared to influence the work reported in this paper.

Highlights

- Highly (0*l*0) preferred orientation aluminum-doped cuprous selenide flexible thin films were fabricated.
- The carrier concentration was successfully adjusted after Al doping, resulting in great enhancement in Seebeck coefficient.
- A record-high figure of merit of 0.76 at 275 °C was achieved due to the high-power factor and low thermal conductivity.
- Further surface organic component coating treatment leads to exceptional flexibility of the thin films.
- The fabricated flexible generator module displays a high-power density of ~5.7 Wm^{-2} at a 20 °C temperature gradient.